

Superdeformation in the Doubly Magic Nucleus ${}^{40}_{20}\text{Ca}_{20}$

E. Ideguchi,¹ D. G. Sarantites,¹ W. Reviol,¹ A. V. Afanasjev,^{2,3,4} M. Devlin,^{1,*} C. Baktash,⁵ R. V. F. Janssens,² D. Rudolph,⁶ A. Axelsson,⁷ M. P. Carpenter,² A. Galindo-Uribarri,⁵ D. R. LaFosse,⁸ T. Lauritsen,² F. Lerma,¹ C. J. Lister,² P. Reiter,² D. Seweryniak,² M. Weiszflog,⁷ and J. N. Wilson,^{1,†}

¹Chemistry Department, Washington University, St. Louis, Missouri 63130

²Physics Division, Argonne National Laboratory, Argonne, Illinois 60439

³Physics Department, University of Notre Dame, Indiana 46556-5670

⁴Laboratory of Radiation Physics, University of Latvia, LV2169, Miera str. 31, Latvia

⁵Physics Division, Oak Ridge National Laboratory, Oak Ridge, Tennessee, 37831-6371

⁶Department of Physics, Lund University, S-22100 Lund, Sweden

⁷The Svedberg Laboratory and Department of Radiation Science, Uppsala University, S-75121 Uppsala, Sweden

⁸Department of Physics and Astronomy, SUNY-Stony Brook, New York 11794

(Received 23 July 2001; published 8 November 2001)

A rotational band with seven γ -ray transitions between states with spin $2\hbar$ and $16\hbar$ has been observed in the doubly magic, self-conjugate nucleus ${}^{40}_{20}\text{Ca}_{20}$. The measured transition quadrupole moment of $1.80^{+0.39}_{-0.29}eb$ indicates a superdeformed shape with a deformation $\beta_2 = 0.59^{+0.11}_{-0.07}$. The features of this band are explained by cranked relativistic mean field calculations to arise from an 8-particle 8-hole excitation.

DOI: 10.1103/PhysRevLett.87.222501

PACS numbers: 21.10.Tg, 21.10.Re, 23.20.Lv, 27.40.+z

Studies of superdeformed (SD) rotational bands in nuclei have been the focus of major experimental and theoretical efforts in the past 15 years. The occurrence of these bands is the manifestation of large shell gaps at a 2:1 axis ratio of the deformed shape for specific particle numbers. Lately, the attention in this field has shifted somewhat from the “traditional” regions of superdeformation at mass numbers 80, 150, and 190 to the lighter nuclei, where protons and neutrons occupy similar orbitals. This trend was initiated by the discovery of superdeformed and highly deformed bands in nuclei near ${}^{56}\text{Ni}$ [1].

Some fascinating aspects of superdeformation in nuclei with $A < 80$ are (i) the appearance of spherical and superdeformed magic numbers at similar particle numbers, which results in dramatic examples of shape coexistence, and (ii) the observation of intense discrete-energy linking transitions between the structures in the second (highly or superdeformed) and the first (spherical or normal-deformed) potential well, including particle decays [1]. This allows for firm spin and parity assignments for the superdeformed bands in most cases. Furthermore, an important consideration for studying these nuclei is that they are amenable to different theoretical treatments that include shell model calculations within a large configuration space [2], quantum Monte Carlo shell model descriptions [3], and a variety of mean field approaches [4,5]. Therefore, these nuclei provide an ideal testing ground to compare and confront these complementary models.

An interesting prospect for a new superdeformed island with similar features as those described above is the region around ${}^{40}_{20}\text{Ca}_{20}$. In this nucleus several relatively low-lying 0^+ states have been observed, which suggests the presence of coexisting shapes, as is the case near other shell closures. Indeed, large transition quadrupole mo-

ments for some of the low-spin states in ${}^{40}\text{Ca}$ have been reported [6], and discussed [7] as multiparticle-multihole deformed excitations.

Early calculations by Gerace and Green [8] explained the low-lying levels of ${}^{40}\text{Ca}$ as a mixture of spherical shell model and deformed states formed by raising particles from the sd to the fp shell. The configurations of the first and second excited 0^+ states (0_2^+ and 0_3^+) were suggested to be 4-particle 4-hole ($4p$ - $4h$) and 8-particle 8-hole ($8p$ - $8h$) excitations, respectively. Recently, Zheng *et al.* [4] using a fixed configuration deformed Hartree-Fock calculation predicted for ${}^{40}\text{Ca}$ an $8p$ - $8h$ SD band with $\beta_2 = 0.599$ starting at 7.08 MeV. If deformed shapes indeed exist in ${}^{40}\text{Ca}$, one should observe rotational bands built on the excited 0^+ states [4,7].

Although a superdeformed band was recently observed in ${}^{36}\text{Ar}$ [9,10], experimental difficulties had so far hampered observation of the highest spin states in ${}^{40}\text{Ca}$. In this Letter, we report the first observation of a superdeformed band extending up to spin 16^+ in the doubly magic self-conjugate nucleus ${}^{40}_{20}\text{Ca}_{20}$.

High-spin states in ${}^{40}\text{Ca}$ were populated via the ${}^{28}\text{Si}({}^{20}\text{Ne}, 2\alpha){}^{40}\text{Ca}$ reaction. A ${}^{20}\text{Ne}$ beam of 84 MeV was provided by the ATLAS accelerator at the Argonne National Laboratory. A thin 0.45 mg/cm^2 ${}^{28}\text{Si}$ target evaporated on a 1.0 mg/cm^2 Ta foil was used. After passing through the Ta foil, the effective beam energy was 80 MeV. The GAMMASPHERE array [11], comprising 101 Compton-suppressed Ge detectors, and the MICROBALL [12], a 4π array of 95 CsI(Tl) scintillation counters, were used to detect γ rays and charged particles, respectively. In this reaction the efficiencies of the MICROBALL for protons and α particles were 68% and 51%, respectively. The charged particles were identified using pulse shape

discrimination on the signals from the CsI(Tl) scintillators. With a trigger condition of three or more Compton-suppressed Ge detectors firing in coincidence, a total of 1.2×10^9 events were collected. From the number of hits in the charged particle detectors, events were sorted into an $E_\gamma - E_\gamma$ coincidence matrix for each evaporation channel. However, the channel selection is limited by the efficiency of the MICROBALL and by the occasional misidentification of charged particle signals. The 2α gated $\gamma - \gamma$ matrix, therefore, contains contaminations from the $2\alpha 1p$ (^{39}K) and $2\alpha 2p$ (^{38}Ar) channels. Their contributions were subtracted to obtain a clean data set for ^{40}Ca .

Some of the high-spin structures in ^{40}Ca have previously been studied [13,14] up to spin 8^+ at 8.1 MeV. An interesting feature of the previous level schemes is the presence of second 0_2^+ and third 0_3^+ states, which are indications of shape coexistence [7]. In our work, the level scheme was extended up to spin 16^+ at 22.1 MeV. Figure 1 shows a partial level scheme for ^{40}Ca , where only positive parity states are reported. An article reporting the complete level scheme is forthcoming [15]. The cascades ending at the levels of 5213 (0_3^+), 3352 (0_2^+), 8103 (8^+), and 6030 (3^+) keV are labeled as bands 1, 2, 3, and 4, respectively. Attention is focused on band 1 with γ -ray transitions be-

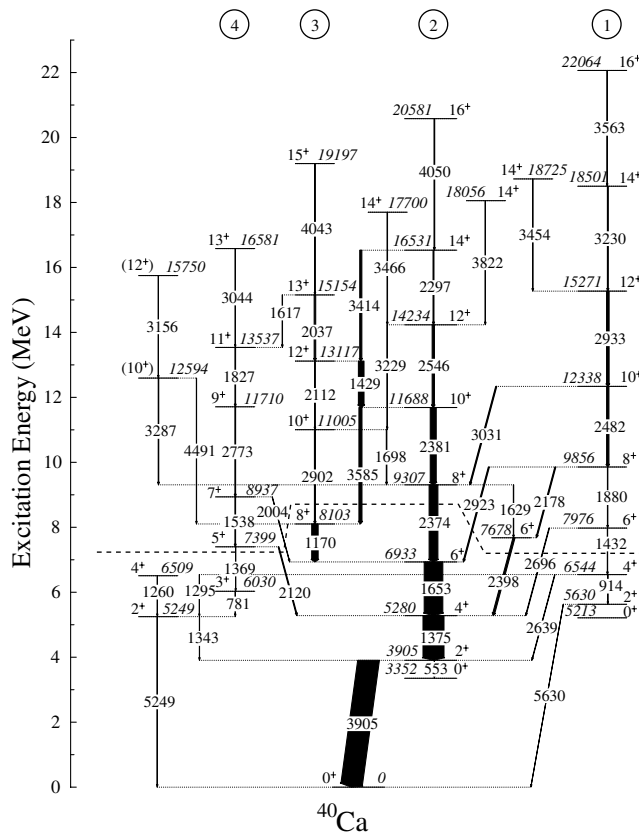


FIG. 1. Partial level scheme of ^{40}Ca ; the energy labels are given in keV, and the widths of the arrows are proportional to the relative intensities of the γ rays. Only the levels below the dashed line were known prior to this work.

tween 914 and 3563 keV. These are highlighted in Fig. 2. Transitions above the 9856 keV level of the band are in coincidence with the previously known transitions of 3905, 1375, and 1653 keV and appear as strong peaks in the spectrum.

Since band 1 is connected to the previously reported fast $E2$ $4^+ \rightarrow 2^+$ transition of 914 keV [$B(E2) = 100$ W.u., $Q_t = 1.69eb$] [7], and linked to the ground state by the 5630 keV transition, it is assigned to be built on the 0_3^+ level. In addition, the newly observed one- and two-step links (\square) to members of band 2 ensure the placement of the individual transitions (\blacktriangledown) in band 1.

Spins of the observed excited levels are assigned on the basis of angular distributions. The multiplicities of the in-band transitions of band 1 and band 2 are found to be consistent with a stretched quadrupole character. The remaining transitions also have a quadrupole character, except for the 2120, 2004, and 2037 keV transitions from the 7399, 8937 (band 4), and 15 154 keV (band 3) levels, respectively, which are dipole in nature. Assuming that the quadrupole transitions correspond to an $E2$ multipolarity, the parity of the excited states is assigned as positive. All states for each spin in band 1 lie at higher excitation than those in band 2 (i.e., band 1 is not “yrast”).

In order to determine the deformation of the bands 1 and 2 in ^{40}Ca , the residual Doppler shifts [16] of the γ -ray energies were measured. The procedure is described in Ref. [17]. The average recoil velocity $\langle\beta\rangle$ is expressed as a fraction of the initial recoil velocity to obtain $F(\tau) \equiv \langle\beta\rangle/\beta_0$. In Fig. 3, the fractional Doppler shifts $F(\tau)$ are plotted as a function of the γ -ray energies. The experimental $F(\tau)$ values are compared with the calculated values based on the known stopping powers from SRIM-2000 [18]. In this calculation the side feeding into each state is

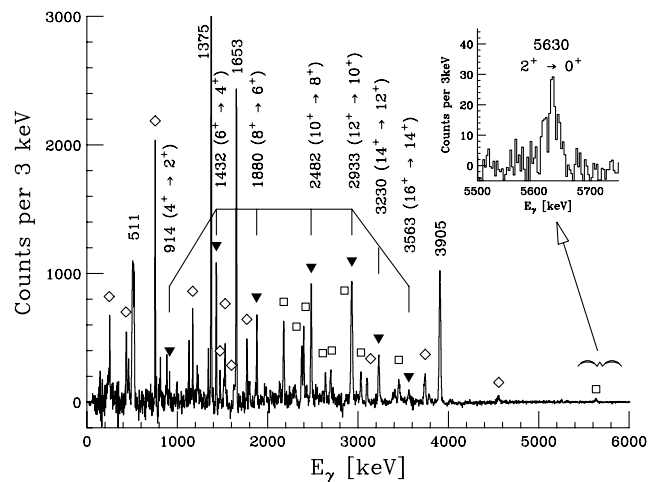


FIG. 2. A γ -ray spectrum obtained by summing coincidence gates set on all members of band 1 (\blacktriangledown) starting from the 2^+ up to the 16^+ state, except for the 1432 keV transition. The \square symbols indicate the transitions decaying from the band. The peaks marked by \diamond are background peaks due to accidental doublets or identified single-escape peaks.

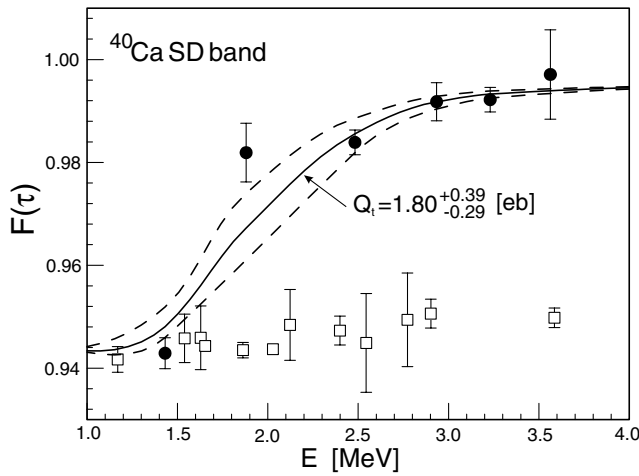


FIG. 3. Fractional Doppler shift $F(\tau)$ as a function of γ -ray energy. Data points for the SD band (filled circles) and other single-particle transitions with similar spins (open squares) are extracted from the residual Doppler shift of the γ -ray energies (see text). The solid line represents $Q_t = 1.80\text{eb}$, and the dashed lines correspond to the quoted uncertainties.

assumed to consist of a cascade of two transitions with the same lifetime as the in-band transitions. The intensities of the side-feeding transitions were modeled to reproduce the observed intensity profile. The data are best fitted with a transition quadrupole moment $Q_t = 1.80^{+0.39}_{-0.29}\text{eb}$. The deduced Q_t value corresponds to a quadrupole deformation of $\beta_2 = 0.59^{+0.11}_{-0.07}$, assuming a rigid axially symmetric rotor. Thus band 1 is associated with a superdeformed shape. Using a similar procedure, the deformation of band 2 was determined from the $Q_t = 0.74 \pm 0.14\text{eb}$ to be $\beta_2 \approx 0.27$.

In the single-particle diagram shown in Fig. 4, in addition to the spherical gap, two prolate and one oblate deformed shell gaps are present at particle number $N = Z = 20$ with values of $\beta_2 \sim 0.6$, ~ 0.3 , and ~ -0.4 ,

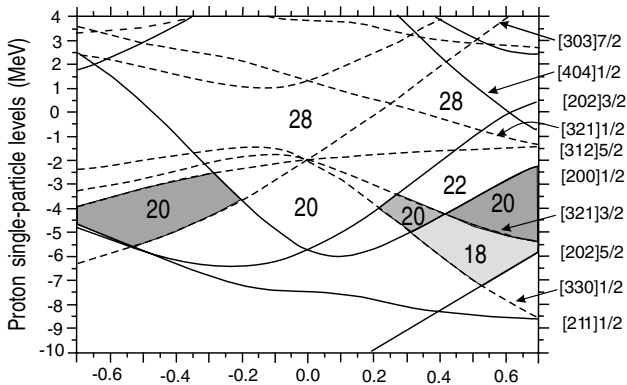


FIG. 4. Woods-Saxon orbitals as a function of the deformation, β_2 , for particle numbers near $N = Z = 20$. The solid and dashed lines are for positive and negative parity orbitals, respectively. Here $\beta_4 = 0$ was assumed. The dark shaded areas indicate the gaps responsible for the larger deformation of band 1 and the smaller deformation of band 2 in ^{40}Ca .

respectively (shaded areas). The gap at $\beta_2 \sim 0.6$ is most likely associated with the SD band 1. The lower deformation gaps at $\beta_2 \sim 0.3$ and $\beta_2 \sim -0.4$ could be responsible for band 2 and could lead to γ softness of the shapes. Directly below the prolate $Z = 20$ gap, another gap is seen with “intermediate” deformation at $N, Z = 18$ (lighter shading). The deformed configuration associated with this gap has been assigned to the $\beta_2 = 0.46 \pm 0.03$ band in ^{36}Ar [9,10].

The pronounced large deformation observed in the rotational band built on the 0_3^+ state is consistent with the multiparticle-multihole nature of this state in the calculations of Refs. [4,8] ($8p\text{-}8h$ excitation). In order to understand the configuration of the observed SD band, we have performed cranked relativistic mean field (CRMF) calculations [19] without pairing employing the NL3 force [20] for the RMF Lagrangian. The results of these calculations are shown in Fig. 5. The SD configuration assigned to band 1 is of the $\pi 3^4\nu 3^4$ type, where the superscripts give the number of protons and neutrons occupying the $N = 3$ ($f_{7/2}$) intruder orbital. That is, the proposed configuration is indeed an $8p\text{-}8h$ excitation. For this configuration the γ deformation is $\sim -10^\circ$ and the $Q_t \approx 2.0\text{eb}$, in close agreement with experiment.

The calculations reproduce reasonably well the trend of the excitation energies as a function of spin and the $J^{(1)}$ moment as a function of rotational frequency, ω . For

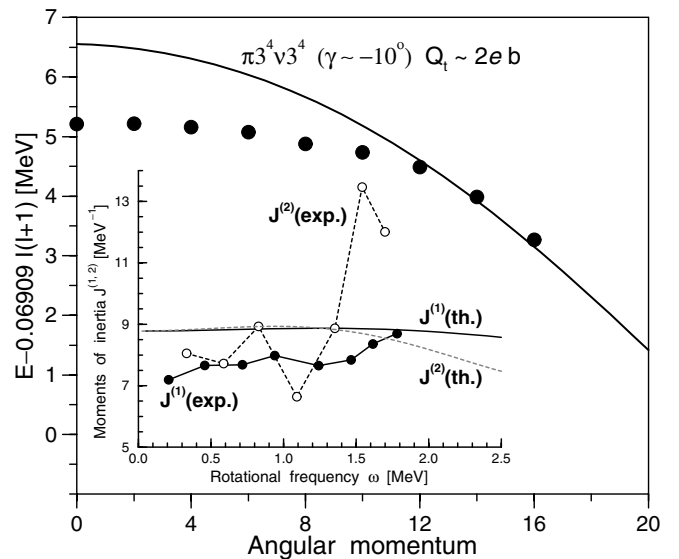


FIG. 5. Excitation energies (E) relative to a rigid rotor energy, $E_{\text{RLD}} = 0.06909I(I + 1)$, as a function of spin. The experimental data for band 1 in ^{40}Ca are shown as unlinked large filled circles, and the results of the CRMF calculations are shown by the solid line. Since pairing is not included, the calculated energies are normalized to the data at high spin. The inset shows the experimental $J^{(1)}$ (filled circles) and $J^{(2)}$ (open circles) values as a function of the rotational frequency for band 1 in ^{40}Ca connected by solid and dashed lines, respectively. The theoretical $J^{(1)}$ and $J^{(2)}$ values from the CRMF calculation are shown for comparison as the solid and dashed smooth lines, respectively.

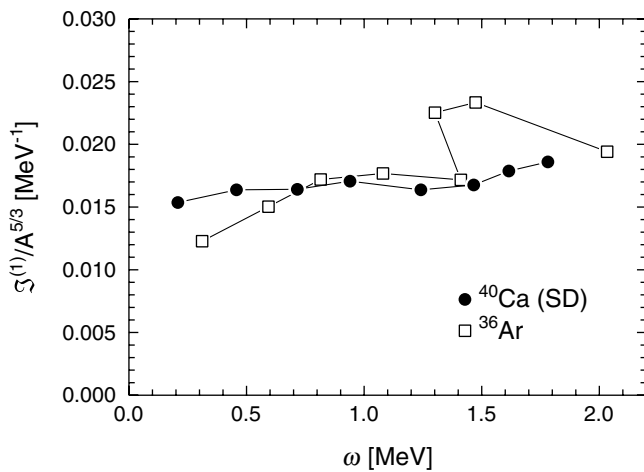


FIG. 6. $J^{(1)}$ moments of inertia scaled by $A^{5/3}$ as a function of rotational frequency for ^{40}Ca and ^{36}Ar .

$\omega \geq 1.5$ MeV, where the alignments of the second pair of $f_{7/2}$ protons and neutrons take place (reflected in a large jump in the dynamic moment of inertia, $J^{(2)}$), the calculated $J^{(1)}$ values are very close to experiment. This suggests that pairing is of minor importance in this frequency range. At lower frequencies (spins), the discrepancy between experiment and calculation consistently points to the need for some pairing. If the pairing would be taken into account, it would lead to the decrease of $J^{(1)}$ at low ω and to the lowering of the calculated $E - E_{\text{RLD}}$ curve at low spin, bringing both calculated quantities in closer agreement with experiment.

The CRMF calculations also give insight into the structure of band 2. This was suggested to correspond to a $4p-4h$ triaxial band [21]. According to the present calculations it is a $\pi 3^2 \nu 3^2$ structure ($4p-4h$ configuration), which will be discussed in detail elsewhere [15]. The presence of many interband transitions between the SD band 1 and band 2 may indicate an overlap in the wave functions for the low and medium spins. Configuration mixing between bands 1 and 2 (or some other band) may also be an explanation for the staggering seen in the $J^{(2)}$ moment of band 1 at low ω (see Fig. 5).

As indicated above, further progress in the description of the new bands requires the introduction of pairing. Unfortunately, unconstrained cranked relativistic Hartree-Bogoliubov (CRHB) calculations [22] converge to the spherical minimum instead of the deformed one, most likely because of a small barrier between the two minima. The implementation of constraints on the Q_{20} and $Q_{2\pm 2}$ moments into the CRHB code [22], which is needed to study the deformed structures, is in progress and the results will be reported later [15].

Finally, Fig. 6 compares the kinematic moments of inertia $J^{(1)}$, for the SD band in ^{40}Ca with that of the rotational band in ^{36}Ar . Below the backbending in ^{36}Ar , the $J^{(1)}$ values of the SD band in ^{40}Ca and in the ^{36}Ar band are similar. The fact that the backbending is observed in ^{36}Ar , but not in ^{40}Ca , is due to both the larger deformation of the latter and the fact that the alignment is connected with the first proton and neutron $f_{7/2}$ pairs in ^{36}Ar and with the second pairs in the SD band of ^{40}Ca .

In summary, a discrete-line superdeformed band has been identified in $^{40}\text{Ca}_{20}$. This is the first observation of an SD rotational structure in a doubly magic spherical nucleus. Its SD character is inferred from a large transition quadrupole moment ($Q_t = 1.80_{-0.29}^{+0.39} \text{eb}$). The properties of the SD band are reasonably well explained by the CRMF calculations without pairing. According to these calculations the SD band is based on an $8p-8h$ excitation in the (sd) (fp) shell. Therefore, this band may be identified as the multiparticle-multihole SD structure that was predicted by shell model calculations more than thirty years ago.

This work was supported in part by the U.S. Department of Energy, Grants No. DE-FG05-88ER40406, No. DE-AC05-00OR22725, No. W-31-109-ENG38, and the Swedish Natural Sciences Research Councils.

*Present address: LANSCE-3, Los Alamos National Laboratory, Los Alamos, New Mexico 87545.

†Present address: NBI, Copenhagen, Denmark.

- [1] D. Rudolph *et al.*, Phys. Rev. Lett. **82**, 3763 (1999).
- [2] E. Caurier *et al.*, Phys. Rev. C **50**, 225 (1994).
- [3] T. Mizusaki *et al.*, Phys. Rev. C **59**, R1846 (1999).
- [4] D. C. Zheng *et al.*, Phys. Rev. C **42**, 1004 (1990).
- [5] A. V. Afanasjev *et al.*, Phys. Rev. C **59**, 3166 (1999).
- [6] P. M. Endt, Nucl. Phys. **A521**, 1 (1990).
- [7] J. L. Wood *et al.*, Phys. Rep. **215**, 101 (1992).
- [8] W. J. Gerace and A. M. Green, Nucl. Phys. **A93**, 110 (1967); **A123**, 241 (1969).
- [9] C. E. Svensson *et al.*, Phys. Rev. Lett. **85**, 2693 (2000).
- [10] C. E. Svensson *et al.*, Phys. Rev. C **63**, 061301(R) (2001).
- [11] I. Y. Lee, Nucl. Phys. **A520**, 641c (1990).
- [12] D. G. Sarantites *et al.*, Nucl. Instrum. Methods Phys. Res., Sect. A **381**, 418 (1996).
- [13] H. P. Leenhouts, Physica (Utrecht) **35**, 290 (1967).
- [14] J. J. Simpson *et al.*, Phys. Rev. Lett. **35**, 23 (1975).
- [15] E. Ideguchi *et al.* (to be published).
- [16] B. Cederwall *et al.*, Nucl. Instrum. Methods Phys. Res., Sect. A **354**, 591 (1995).
- [17] F. Lerma *et al.*, Phys. Rev. Lett. **83**, 5447 (1999).
- [18] J. F. Ziegler, <http://www.research.ibm.com/ionbeams>
- [19] A. V. Afanasjev *et al.*, Nucl. Phys. **A608**, 107 (1996).
- [20] G. A. Lalazissis *et al.*, Phys. Rev. C **55**, 540 (1997).
- [21] W. J. Gerace *et al.*, Nucl. Phys. **A285**, 253 (1977).
- [22] A. V. Afanasjev *et al.*, Nucl. Phys. **A676**, 196 (2000).